Journal of Materials Chemistry A

Accepted Manuscript

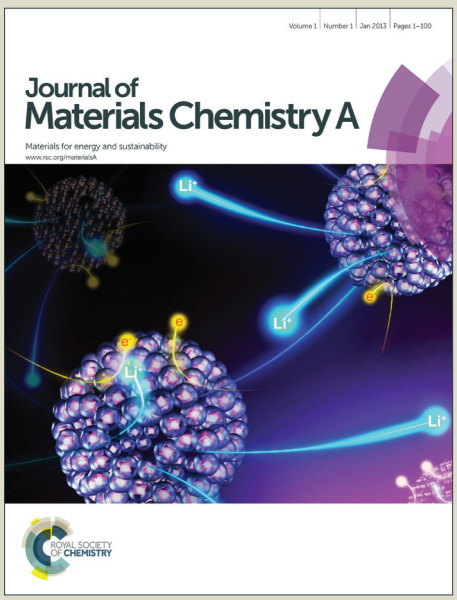

ROYAL SOCIETY OF CHEMISTRY

www.rsc.org/materialsA

Cite this: DOI: 10.1039/c0xx00000x

www.rsc.org/xxxxxx

ARTICLE TYPE

Multiple Heteroatoms Induced Carrier Engineering and Hierarchical Nanostructure for High Thermoelectric Performance of Polycrystalline $In_4Se_{2.5}$

Yubo Luo, Junyou Yang*, Ming Liu, Ye Xiao, Liangwei Fu, Weixin Li, Dan Zhang, Mingyang Zhang, Yudong Cheng

Received (in XXX, XXX) Xth XXXXXXXXX 20XX, Accepted Xth XXXXXXXXX 20XX
DOI: 10.1039/b000000x

In this paper, different atom combinations of Pb, I and Cu have been doped into the $In_4Se_{2.5}$ matrix and a systematic investigation has been carried out to the synergistic effect of multiple heteroatoms on the microstructure and thermoelectric properties of polycrystalline $In_4Se_{2.5}$. By this approach, the electron and phonon transport properties are rationally regulated, the electrical conductivity increases greatly due to the multiple doping, which result in an simultaneous increase of carrier concentration and mobility. The Seebeck coefficent also maintains at the relative high level in high temperature range due to the energy-dependent electron scattering at the metal nanoparticles/matrix interfaces. In addition, the lattice thermal conductivity is also greatly reduced because of the wide frequency phonon scattering by the point defects and hierarchical metal nanoparticles combined with the phonon-phonon interactions. Consequently, an enhancement to the ZT with a maximum of 1.4 (723K) has been achieved in the multiple doped $In_4Se_{2.5}$ sample.

Introduction

Owing to the potential capability to directly convert the waste heat of automobile exhaust and various industrial processes into electricity, thermoelectric (TE) materials have been receiving more and more attention from researchers in recent years. Usually, TE conversion efficiency is determined by the dimensionless figure of merit $ZT=S^2T/\rho\kappa$, where S is the Seebeck coefficient, ρ the electrical resistivity, κ the thermal conductivity and T the absolute temperature, respectively. However, the "counter-indicated" relationship of these properties (S, ρ, κ) poses the greatest challenge to develop high ZT TE materials.[1] Over the past 15 years, remarkable progresses have been made in improving the ZT value by lowering the lattice thermal conductivity (κ_l) while minimizing the reduction of power factor ($S^2\sigma$) through introduction of nanostructure into TE materials.[2-4] Nevertheless, a good TE material should also has high electrical conductivity to minimize the Joule heat and high Seebeck coefficient to maximize the conversion of heat to electrical power.[5] As a consequence, improving the power factor ($S^2\sigma$) has been considered as a promising strategy to enhance the TE performance for the next generation TE materials,[6] and this can be achieved in general by rationally regulating the electronic transport properties within a bulk matrix, such as the alteration of chemical composition and quantum dot engineering.[7]

As a new chalcogenide TE material, In_4Se_3 is very compelling because of its natural nanowire-like cylindrical clusters and quasi-one-dimensional indium chains at the cleavage (100) surface, which make it possess an instinctive low lattice thermal conductivity and high Seebeck coefficient, and a remarkable ZT=1.48 at 705K for single crystal $In_4Se_{2.35}$ has been reported by Rhyee et al.[8] Since then, increasing research activities have been focused on this layered structure single crystal material and a high ZT=1.53 has been obtained at 698K for $In_4Se_{2.67}Cl_{0.03}$ single crystal.[9,10] However, single crystal In_4Se_3 is prone to cleave because of the weak van der Waals bonding between the b-c layers, and a randomly oriented polycrystalline microstructure will be more preferable for practical application if its TE properties are comparable to those of In_4Se_3 single crystal from the standpoint of mechanical performance. Therefore, more and more attention has been paid on polycrystalline In_4Se_3 based TE materials and encouraging results have been present successionally.[11-16] Recent report showed that the lattice thermal conductivity of polycrystalline In_4Se_3 based thermoelectric materials could be reduced drastically by introducing nanoscale secondary phase and a high ZT value was thus achieved by Lin.[17] Even so, the power factor of polycrystalline In_4Se_3 based TE materials is yet unparallel with their single crystal counterparts, thereby, improving the power factor with minimum increment of the thermal conductivity should be the next research target of the polycrystalline In_4Se_3 based TE materials.

As typically exampled in skutterudites and some other TE materials,[18-21] dual even multiple doping turns out to be an effective way to improve their power factors as well as reduce thermal conductivities due to the complex multiple effects. For In_4Se_3 materials, there are four different In sites and three different Se sites in its unique lattice structure (*Pnnm* space group), which provides abundant chemical environment distinguishable atom sites, therefore multiple possibilities for anion and/or cation substitution and intercalation to regulate the TE performance of In_4Se_3-based materials. Up to now, however, less dual doping and even no multiple doping related work has been reported for polycrystalline In_4Se_3 based materials yet. In this work, we investigated systematically the synergistic effects

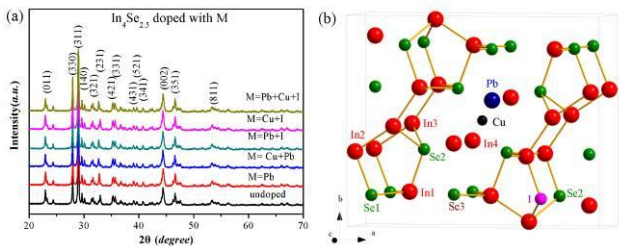

Figure 1. (a), XRD patterns for the un-doped and doped $In_4Se_{2.5}$ (PDF# 01-083-0039) (b), the energetically favorable sites for each heteroatom in the crystal structure of In_4Se_3.

of multiple heteroatoms on the microstructure and thermoelectric properties of polycrystalline $In_4Se_{2.5}$ by doping with Pb, Pb/I, Pb/Cu, Cu/I and Pb/Cu/I, respectively. An enhanced power factor which is superior to its counterpart of single crystal $In_4Se_{2.67}Cl_{0.03}$, and a suppressed lattice thermal conductivity has been achieved in the polycrystalline $In_4Se_{2.5}$ sample by elaborate manipulation of carrier concentration and mobility and phonon scattering through multiple doping. As a result, the ZT value has been improved by dual and multiple doping, and a highest ZT of 1.4 is obtained at 723K for the multiple-doped polycrystalline $In_4Se_{2.5}$, which is comparable to its single crystal counterpart and some other high performance TE materials such as Bi_2Te_3,[22] $(Zr_{0.5}Hf_{0.5})_{0.5}Ti_{0.5}NiSn_{1-y}Sb_y$,[23] and β-$Zn_4Sb_3$[24] compounds.

Experimental Section

Preparation: Stoichiometric quantities of the raw materials weighted with composition of $In_4Se_{2.5}$, $In_4Se_{2.5}$+M (0.8 at%) from In(99.99%), Se(99.99%), Cu(99.99%), Pb(99.9%) and I_2(99.9%) were loaded into quartz tubes followed by mixing. Then the tubes were evacuated (10^{-1} Pa), sealed and slowly heated up to 823K and kept for 24h with regular rocking to ensure a uniform distribution of composition, then quenched into cooling water. After that, the obtained ingots were grinded to powders and further annealed for 24h at 693K then cooled to room temperature naturally. Finally the prepared sample powders were hot pressed at 723K for 2h under a pressure of 120MPa in a purified Argon atmosphere to get disk bulk samples.

Characterization and Measurements: The phase purity and characterization of powder specimens were recorded on a Philip X'Pert X-ray diffractometer equipped with Cu Kα radiation (λ=0.15418nm). The morphologies of specimen fractographs of bulk samples were observed by a field-emission scanning electron microscope (FESEM) (NanoSEM 450) with the Schottky field emission and acceleration voltage of 10 kV. High resolution transmission electron (HRTEM) images and energy dispersive x-ray spectroscopy (EDS) microanalysis were performed by a transmission electron microscope (JEM-2100) in bright-field mode with an acceleration voltage of 200 kV. Seebeck coefficient and electrical resistivity were simultaneously measured in a custom designed apparatus (Namicro-III). Thermal conductivity is calculated in the light of κ=DCpλ, here, the density (D) was determined by the Archimedes' method, the specific heat capacity (Cp) was derived by differential scanning calorimeter

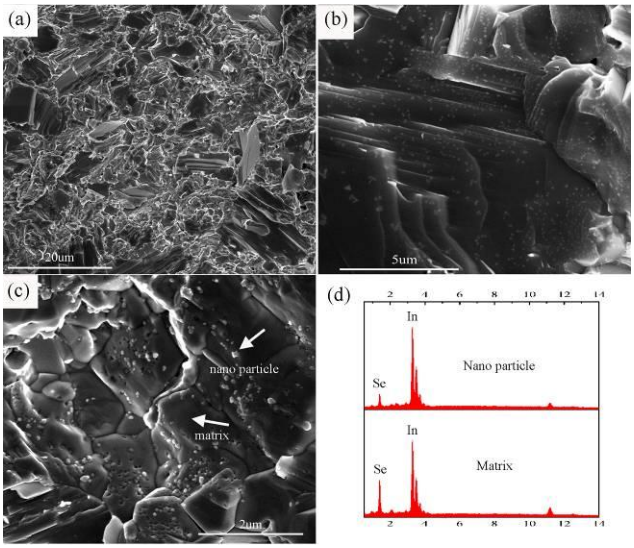

Figure 2. (a-c), Low and high magnification FESEM fractographs of the multiple doped $In_4Se_{2.5}$ sample; (d) EDS composition analysis of the matrix and one of the nanoparticles marked with the arrows in the multiple doped $In_4Se_{2.5}$ sample.

(PerkinElmer DSC7) and the thermal diffusivity λ was measured by a Netzsch laserflash diffusivity instrument (LFA 457). The Hall measurements were accomplished by Van der Pauw method in a Hall effect measurement system (HMS 5500). To avoid the inconsistency due to the possible texture though it is less obvious in our samples, all of the above electrical and thermal properties were measured in the perpendicular to the pressing direction of the pellet.

Results and discussion

Powder X-ray Diffraction and Crystal Structure

The synthesis of all samples is rather straightforward by melting and leads to a single phase as illustrated by the corresponding powder X-ray diffraction data in Figure 1a, which can be well indexed as In_4Se_3 with the JCPDS# 083-0039 file. No peak of any secondary phase has been observed within the detection limit of powder XRD, indicating that these samples maintain the crystal structure of In_4Se_3 even in the existence of selenium deficiency and various doping heteroatoms. Noteworthily, no obvious preferential orientation was observed in the samples, as demonstrated in Figure S1. Figure 1b illustrates the crystal structure of In_4Se_3 and the energetically favorable sites for each heteroatoms, where Pb substitutes the In_4 site (Ref.17), I replaces the Se_2 site [25] while Cu occupies an intercalation position (Ref.16). Theoretically, once they solve into the lattice of In_4Se_3 and occupy the abovementioned sites, all of them will act as donors and result in an increment of carrier concentration according to the following equation:

$$Pb \xrightarrow{In_4Se_3} Pb'_{In_4} + e^{\bullet}$$

$$I \xrightarrow{In_4Se_3} I'_{Se_2} + e^{\bullet}$$

$$Cu \xrightarrow{In_4Se_3} Cu'_{Int} + e^{\bullet}$$

Microstructure Observation

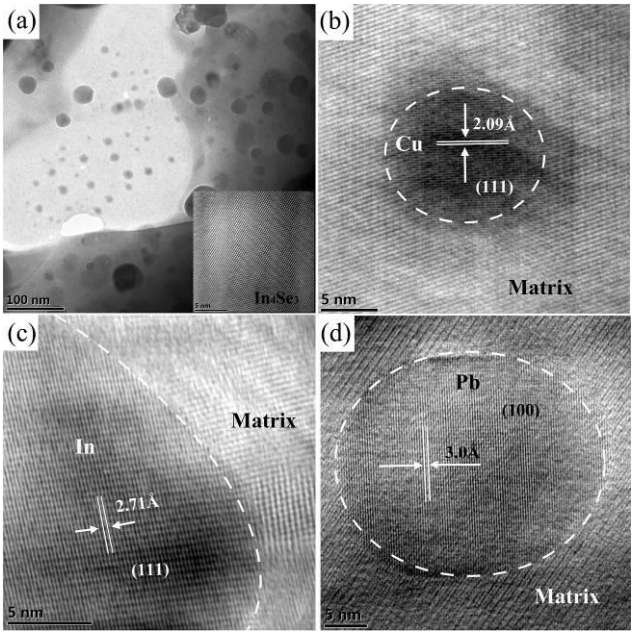

Figure 3. (a), Low magnification TEM image of the multiple doped $In_4Se_{2.5}$ sample; (b-d), the HRTEM images of Cu, In and Pb nanoparticles with d_{Cu111}=2.09 Å, d_{In111}=2.71 Å and d_{Pb100}=3.0 Å, respectively.

Field emission scanning electron microscopy (FSEM) on the fractographs of the multiple doped $In_4Se_{2.5}$ sample reveals a typical polycrystalline microstructure with sub-micron randomly oriented grains as displayed in Figure 2a. Noteworthily, dispersive particles about tens of nanometer in size distributed in the matrix can be apparently observed in the high magnification micrographs (Figure 2b and 2c). The EDS composition analysis (Figure 2d) indicates that these nanoparticles are the surplus metallic indium precipitates, which is consistent with the In-Se binary phase diagram (Figure S2) and the earlier reports of Se-deficiency In_4Se_{3-x} (Ref.15).

In order to further understand the microstructure of the samples, high resolution transmission electron microscope (HRTEM) observation was carried out and a systematic investigation was performed to the samples. It also reveals that there are some nanoparticles in the samples. Figure 3a displays a typical TEM image of the Pb/Cu/I multiple-doped sample, it can be seen that there are many nanoscale particles about several to dozens of nanometers in the matrix. HRTEM images (Figure 3b-d) and the EDS composition analysis (Figure S3) confirm that these hierarchical nanoparticles are primarily of Cu, Pb and In precipitates, and the interfaces between the nanoinclusions and matrix are obviously incoherent owing to the large difference of crystal structure between them. It is noteworthy that these precipitates are nanoscale and dispersive, furthermore, they are tiny in amount, therefore no peak of them has been observed in the XRD patterns. Among them, Cu nanoparticles come from the undissolved elemental copper because of the small solid solubility (about 0.2%) of Cu in In_4Se_3 lattice,[26] meanwhile, the solid solubility of Pb in the matrix decreases with the co-doping of other heteroatoms thus resulting in the supersaturation and precipitation of Pb in the matrix, although the doping amount is

Electrical Properties

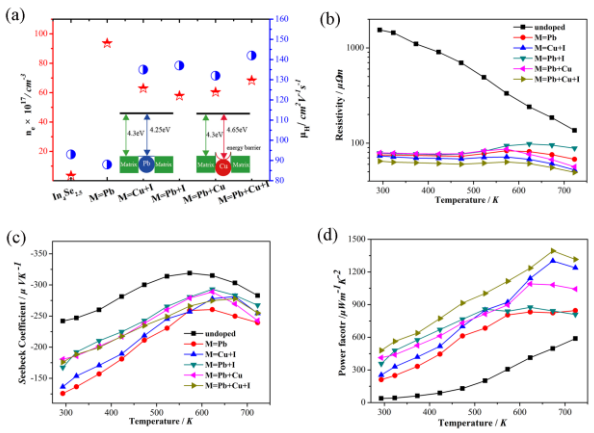

Figure 4. (a), The carrier concentration and mobility of the samples and an inset of the schematic diagram of energy filter; (b-d), the temperature dependence of the electrical resistivity (ρ), the Seebeck coefficient (S), and the power factor for the un-doped/doped $In_4Se_{2.5}$.

lower than the solid solubility limit (0.75 at.%) of Pb in In_4Se_3 (Ref.17), that is why Pb nanopartilces were also observed. The carrier concentration and mobility were measured by Hall effect at room temperature and shown in Figure 4a. In compared to the undoped $In_4Se_{2.5}$ matrix, the Pb mono-doped sample shows higher carrier concentration and lower mobility, and this is well agreement with the other reports[27, 28] that the introduction of donor impurities into an n-type semiconductor leads to a drastic increase in the carrier density while the additional ionized impurity scattering and enhanced carrier scattering deteriorates the carrier mobility. However, the simultaneous increase of carrier concentration and mobility after dual and multiple doping make it paradoxically. Basically, the mobility (μ) is inversely proportional to the carrier effective mass (m*) according to the relaxation time (τ) approximation: $\mu=q\tau/m^*$, and the increase of carrier mobility in the dual and multiple doped samples means the decrease of effective mass m*. Therefore, the unusual increment of the carrier mobility in the system can be attributed to the following reasons: 1) Iodine substitution for Se site. The mobility enhancement caused by iodine subsitiution for Se was also observed elsewhere (Ref. 25), although the mechanism is still unclear owing to the complex carrier scattering behavior combined of acoustic phonon scattering and ionized impurity scattering caused by iodine substitution for Se site. 2) The energy-dependent scattering, mainly originating from the energy barrier at the interfaces between the metal Cu nanoparticles and the matrix, because of the higher work functions of Cu (4.65eV) than In_4Se_3 (4.30ev) as illustrated in the insert of Figure 4a, which acts as an energy filter for low energy electrons while high energy and high mobility electrons are unaffected. Besides, the enhanced S of the multiple doped samples at high temperature (Fig. 4c) also suggests that the electron that contributes to the electronic transport is skewed to higher energy. that is why the carrier concentration of the Pb/Cu dual doped samples are lower than that the Pb mono-doped one while the mobility is on the contrary. Analogous results have also been reported recently in the full-Heusler quantum dot embedded half-Heusler alloys (Ref. 7, 28) and $AgSbSe_2$-ZnSe compounds.[29]

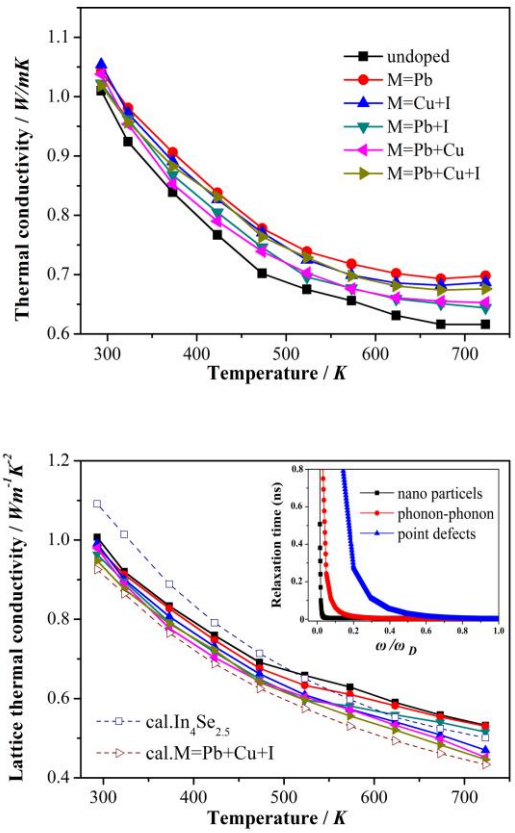

Figure 5. (a), Temperature dependence of the total thermal conductivity κ of all the samples; (b), temperature dependence of the lattice thermal conductivity κ_l of all the samples and the relaxation time versus the normalized frequency of multiple doped $In_4Se_{2.5}$ at room temperature, the phonon frequency (ω) is normalized to the Debye frequency (ω_D).

The typical temperature dependence of the electrical resistivity (ρ) of all samples was presented in Figure 4b. It can be seen that the electrical resistivity of $In_4Se_{2.5}$ is conspicuously reduced by doping throughout the whole testing temperature range, especially at the low temperature stage. As ρ is close related with the carrier concentration (n) and mobility (μ): $\rho=1/ne\mu$, thereby, the reduction of ρ should be attributed to the sharply changed carrier concentration and mobility by dual/multiple doping. In addition, the electrical resistivity of the doped samples show a heavily doped semiconductor behavior before the intrinsic excitation begins to take effect in the low temperature range and decreases with further raising the temperature, while the undoped sample shows a typical semiconductor behaviour during the measurement temperature, as observed in reference 16. The negative Seebeck coefficient (S) (Figure 4c) indicates that all these samples are of n-type conduction with electrons as the major carriers, and it follows a nearly linear temperature dependence up to the maximum value and then slightly decreases with a further increase of temperature for all samples. However, the Seebeck coefficients of the doped samples are obviously below the value of the undoped $In_4Se_{2.5}$, according to the Mott expression,[30] Seebeck coefficient is dependent on the energy derivative of the energy-dependent carrier concentration and mobility taken at the Fermi energy by the following equation:

$$S = \frac{\pi^2 k_B^2 T}{3q}\left(\frac{dn(E)}{ndE} + \frac{d\mu(E)}{\mu dE}\right)_{E=E_F}$$

where k_B is Boltzmann's constant. Therefore, the Seebeck coefficient of the doped samples are generally lower than the undoped $In_4Se_{2.5}$ as a consequence of the increased carrier concentration. Even so, the Seebeck coefficient of the dual and multiple doped samples still maintains at the relative high level in high temperature range due to the energy-dependent electron scattering at the metal nanoparticles/matrix interfaces as mentioned above.

The slight decrease of thermopower and a large reduction in the electrical resistivity result in large increase in the power factor (S^2/ρ) of all the doped samples (Figure 4d). At room temperature, the S^2/ρ of $In_4Se_{2.5}$ is only 38μWK^{-2} and it slowly increases with temperature to 588μWK^{-2} at 723K. However, the power factor shows an increment at different degree in the doped samples at all temperature and the largest enhancement of power factor was obtained in the Pb/Cu/I multidoped compound, which presents a maximum PF of 1394μWK^{-2} at 673K and drop to 1319 μWK^{-2} at 723K. It increases more than two times (at 723K) in comparison to the undoped $In_4Se_{2.5}$ matrix, and it is even higher than that of the $In_4Se_{3-x}Cl_{0.03}$ single crystal (Ref. 9) as well as other polycrystalline In_4Se_3 based samples.

Thermal Transport Properties

The thermal conductivity κ of the samples was shown in Figure 5a and it declines with increasing temperature in the range of 293–723K. The lattice thermal conductivitiy κ_l of all the samples, shown in Figure 5b, was estimated by subtracting the electronic part κ_e from κ. Here, κ_e is calculated by Wiedemann−Franz law $\kappa_e = LT\sigma$, where L is the Lorenz number, which was eitimated by the reduced Fermi energy and scattering parameter[31] as detailed represented in SI4. From the calculated κ_l, an obvious reduction of κ_l was observed in the doped samples when compared to the undoped $In_4Se_{2.5}$ matrix. As known, the lattice thermal conductivity mainly depends on the integration of the relaxation times from various scattering processes based on the Callaway mode.[32]

$$k_l = \frac{K_B}{2\pi^2 \upsilon}\left(\frac{K_B T}{\hbar}\right)^3 \int_0^{\theta_D/T} \tau(x)\frac{x^4 e^x}{\left(e^x-1\right)^2}dx$$

Where $\hbar$ is the reduced plank constant, θ is the Debye temperature, υ is the phonon velocity, χ is the usual dimensionless variable $\hbar\omega/k_BT$ and τ is the phonon relaxation time. As the phonon relaxation time is mainly related to scattering from multiple scatteirng centers in the materials, according to Matthiessen's rule, τ can be written as:

$$\tau^{-1} = \tau_{PD}^{-1} + \tau_{NP}^{-1} + \tau_{p-p}^{-1} + \tau_B^{-1}$$

here, τ_{PD}, τ_{NP}, τ_{p-p}, τ_B are the relaxation times crrespond to scattering from point defect, nanoparticles, phonon-phonon interactions and boundaries/interfaces, respectively. For our samples, the reduction of lattice thermal conductivity in the doped samples should be attributed to the three primary scattering terms: the point defect scattering, the nanoparticle scattering and the phonon-phonon scattering based on the microstructure and

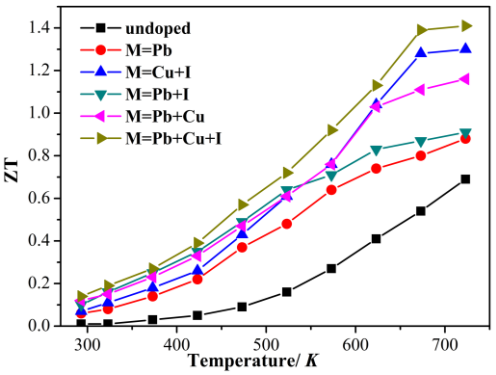

Figure 6. ZT values of the undoped and doped $In_4Se_{2.5}$ samples.

composition analysis, and their relaxation times were calculated as follows.

The point defect scattering, mainly due to the solution of heteroatoms (Pb,Cu and I) in the matrix, can be expressed as[33]

$$\tau_{PD}^{-1} = \frac{V_0}{4\pi\upsilon^3}\Gamma\omega^4$$

Where V_0 is the average volume per atom, υ is the average lattice sound velocity and Γ is the disorder scattering parameter depending on the mass fluctuations. The nanoparticles' contribution to the relaxation time was estimated by using a Mathiessen type interpolation between the short and long wavelength scattering regimes, [34-37]

$$\tau_{NP}^{-1} = \upsilon(\sigma_s^{-1} + \sigma_l^{-1})^{-1}V_P$$

Where Vp is the density of nanoparticles, σ_s and σ_l are the cross section limits given by

$$\sigma_l = \frac{4}{9}\pi R^2\left(\frac{\Delta D}{D}\right)^2\left(\frac{\omega R}{\upsilon}\right)^4$$

Where R is the average size of particle, D is the corresponding mass density, ΔD is the mass density difference between the nanoscale particle and the matrix, and ω is phonon frequency.

The relaxation time of phonon-phonon Umklapp processes, based on the suggestion of Slack and Galginaitis,[38] is expressed as

$$\tau_U^{-1} = \frac{\hbar\gamma^2\omega^2 T}{M\upsilon^2\theta}e^{-\theta/3T}$$

Where M is the average mass of an atom in the crystal, γ is the Grüneisen parameter, θ is the Debye temperature and ν is the phonon velocity.

And the relaxation time of normal phonon-phonon scattering is given by[39]

$$\tau_N^{-1} = \beta\tau_U^{-1}$$

where β is the ration of normal phonon scattering to Umklapp scattering. On the basis of the above formulas and the parameters obtained from TEM observations and reference 10 (SI Table1), the calculated relaxation time dependence on phonon frequency of the above three main terms were shown in Figure 5b (inset) and the calculated lattice thermal conductivity of $In_4Se_{2.5}$ and pb/Cu/I doped $In_4Se_{2.5}$ based on the Callaway mode was plotted in Figure 5b.

The theoretical calculation shows clearly that the intermediate to high frequency phonon are mostly affected by the atomic scale point defects and the Umklapp scattering, while the low frequency phonon are mainly scattered by the introduced metal nanoparticles. Therefore resulting in the greatly reduction to the lattice thermal conductivity in the dual/multiple doped samples as both observed in the experimental and calculated results.

Thermoelectric Performance

A gradient improved figure of merit ZT, resulted from the combination of the measured electrical and thermal transport properties over the range 293−723 K, of the Pb, Pb/I, Pb/Cu, Cu/I and Pb/Cu/I doped samples along with the $In_4Se_{2.5}$ matrix was obtained and shown in Figure 6. The ZT value increases with temperature for all the doped samples and the maximum ZT reaches 1.4 for the multi-doped sample at 723K, which is even comparable to the state-of-the-art single crystalline In_4Se_3-based materials. The enhancement of thermoelectric performance should be mainly attributed to the great increase in the power factor due to the multiple effects. It also indicates a feasible strategy that the TE properties a materialcould be remarkably improved by a synergistic regulation to both electron and phonon transport through a rational introduction of multiple heteroatoms.

Conclusions

In summary, a series of differently doped $In_4Se_{2.5}$ samples have been prepared in this work. A unique microstructure with hierarchical nanoparticles, originating from the nonstoichiometric $In_4Se_{2.5}$ matrix and the supersaturated precipitation of the multiple-doped heteroatoms, has been formed and a synergistic regulation on the electron and phonon transport properties has been realized in this compound, this is because: (1) The simultaneous increase in the carrier concentration and the mobility stem from the multiple atoms doping, which results in an large increase in the electrical conductivity; (2) The "effective" electron concentration decreases significantly due to the energy-dependent scattering at the metal nanoinclusions - matrix interfaces because of the different work function between nanoinclusions and matrix, which results in simultaneous increase of carrier concentration and mobility and slight decrease in the Seebeck coefficient at high temperature range; (3) The lattice thermal conductivity has also been greatly reduced because of additional phonon scattering caused by the introduced metal nanoparticles and point defects, result in a wide frequency phonon scattering by combining with the phonon-phonon interactions scattering. By this approach, an enhanced power factor which is superior to its counterpart of single crystal $In_4Se_{2.67}Cl_{0.03}$ was obtained and a significant enhancement to the ZT with a maximum of 1.4 (723K) has been achieved in the multiple doped $In_4Se_{2.5}$.

Acknowledgements

This work is co-financed by National Basic Research Program of China (Grant No.2013CB632500), National Natural Science

Foundation of China (Grant No. 51272080 and 51072062), Open Fund of State Key Laboratory of Advanced Technology for Materials Synthesis and Processing, Wuhan University of Technology (No. 2013-KF-3). The technical assistance from the Analytical and Testing Center of HUST is also gratefully acknowledged.

Notes and references

State Key Laboratory of Materials Processing and Die & Mould Technology, Huazhong University of Science and Technology, Wuhan 430074, P. R China

Fax/Tel: +86-27-87558310; E-mail: jyyang@mail.hust.edu.cn

† Electronic Supplementary Information (ESI) available: [details of any supplementary information available should be included here]. See DOI: 10.1039/b000000x/

1 J. P. Heremans, B. Wiendlocha, A. M. Chamoire, Energy Environ. Sci., 2012, **5**, 5510.
2 G. J. Snyder, E. S. Toberer, Nature Materials, **2008**, **7**, 105.
3 Y. Xiao, J. Yang, G. Li, M. Liu, L. Fu, Y. Luo, W. Li, J. Peng, Intermetallics, 2014, **50**, 20.
4 L. Fu, J. Yang, Y. Xiao, J. Peng, M. Liu, Y. Luo, G, Li, Intermetallics, 2013, **43**, 79.
5 G. Zhang, Q. Zhang, C. Bui, G. Q. Lo, B. Li, Appl. Phys. Lett., 2009, **94**, 23108.
6 Y. Lan, A. J. Minnich, G. Chen, Z. Ren, Adv. Funct. Mater., 2010, **20**, 357.
7 Y. Liu, P. Sahoo, J. P. A. Makongo, X. Zhou, S. kim, H. Chi, C. Uher, X. Pan, P. F. P. Poudeu, J. Am. Chem. Soc., 2013, **135**, 7486.
8 J. Rhyee, K. H. Lee, S. M. Lee, E. Cho, S. I. Kim, E. Lee, Y. S. Kwon, J. H. Shim, G. Kotliar, Nature. 2009, **459**, 965.
9 J. Rhyee, K. Ahn, K. H. Lee, H. S. Ji, J. Shim, Adv. Mater., 2011, **23**, 2191.
10 H. S. Ji, H. Kim, C. Lee, J. Rhyee, M. H. Kim, Physical Review B, 2013, **87**, 125111.
11 X. Shi, J. Y. Cho, J. R. Salvador, J. Yang, H. Wang, Appl. Phys. Lett., 2010, **96**, 162108.
12 G. H. Zhu, Y. C. Lan, H. Wang, G. Joshi, Q. Hao, G. Chen, Z. F. Ren, Physical Review B, 2011, **83**, 115201.
13 J. Yang, J. Wu, G. Li, J. Zhang, J. Peng, Journal of Electronic Materials, 2012, **41**, 1077.
14 G. Li, J. Yang, Y. Luo, Y. Xiao, L. Fu, M. Liu, J. Peng, J. Am. Ceram. Soc., 2013, **96**, 2703.
15 Y. Zhai, Q. Zhang, J. Jiang, T. Zhang, Y. Xiao, S. Yang, G. Xu, J. Mater. Chem. A, 2013, **1**, 8844.
16 Y. Luo, J. Yang, G. Li, M. Liu, Y. Xiao, L. Fu, W. Li, P. Zhu, J. Peng, S. Gao, J. Zhang, Adv. Energy Mater., 2014, **4**, 1300599
17 Z. Lin, L. Chen, L. Wang, J. Zhao, L. Wu, Adv. Mater, 2013, **25**, 4800.
18 Y. O. T. Iida, T. Sakamoto, R. Miyahara, A. Natsui, K. Nishio, Y. Kogo, N. Hirayama, Y. Takanashi, Phys, Status, Solidi C, 2013, **10**, 187.
19 H. Wang, Z. M. Gibbs, Y. Takagiwa, G. J. Snyder, Energy Environ. Sci., 2014, **7**, 804.
20 S. Ballikaya, N. Uzar, S. Yilidirim, J. R. Salvador, C. Uher, Journal of solid state chemistry, 2012, **193**, 31.
21 X. Shi, J. Yang, J. R. Salvador, M. Chi, J. Y. Cho, H. Wang, S. Bai, J. Yang, W. Zhang, L. Chen, J. Am. Chem. Soc., 2011, **133**, 7837.
22 B. Poudel, Q. Hao, Y. Ma, Y. Lan, A. Minnich, B. Yu, X. Yan, D. Wang, A. Muto, D. Vashaee, X. Chen, J. Liu, M. S. Dresselhaus, G. Chen, Z. Ren, Science, 2008, **320**, 634.
23 S. Sakurada, N. Shutoh, Appl. Phys. Lett., 2005, **86**, 082105.
24 J. Lin, X. Li, G. Qiao, Z. Wang, J. Carrete, Y. Ren, L. Ma, Y. Fei, B. Yang, L. Lei, J. Li, J. Am. Chem. Soc., 2014, **136**, 1497.
25 K. Ahn, E. Cho, J. Rhyee, S. I. Kim, S. Hwang, H. Kim, S. M. Lee, K. H. Lee, J. Mater, Chem. 2012, **22**, 5730
26 P. V. Galiy, A. V. Musyanovych, Y. M. Fiyala, Physica E, 2006, **35**, 88.
27 C. J. Vineis, A. Shakouri, A. Majumdar, M. G. Kanatzidis, Adv. Mater., 2010, **22**, 3970.
28 J. P. A. Makongo, D. k. Misra, X. Zhou, A. Pant, M. R. Shabetai, X. Su, C. Uher, K. L. Stokes, P. F. P. Poudeu, J. Am. Chem. Soc., 2011, **133**, 18843.
29 S. N. Guin, D. S. Negi, R. Datta, K. Biswas, J. Mater. Chem. A, 2014, **2**, 4324.
30 J. P. Heremans, V. Jovovir, E. S. Toberer, A. Saramat, K. Kurosaki, A. Charoenphakdee, S. Yamanaka, G. J. Snyder, Science, 2008, **321**, 554.
31 W. Liu, Q. Zhang, Y. Lan, S. Chen, X. Yan, Q. Zhang, H. Wang, D. Wang, G. Chen, Z. Ren, Adv. Energy Mater., 2011, **1**, 577.
32 J. Callway, Phys. Rev., 1961, **122**, 787.
33 J. Callaway, H. C. Vonbaeyer, Phys. Rev., 1960, 120, 1149.
34 C. B. Vining, J. Appl. Phys., 1991, **69**, 331.
35 N. Mingo, D. Hauser, N. P. Kobayashi, M. Plissonnier, A. Shakour, Nano Lett., 2009, **9**, 711.
36 J. He, J. Androulakis, M. G. Kanatzidis, V. P. Dravid, Nano Lett., 2012, **12**, 343.
37 J. He, S. N. Girard, J. Zheng, L. Zhao, M. G. Kanatzidis, V. P. Dravid, Adv. Mater., 2012, **24**, 4440.
38 D. T. Morelli, J. P. Heremans, Physical Review B, 2002, **66**, 195304.
39 E. F. Steigmeier, B. Abeles, Phys. Rev., 1964, **136**, A1149.

Highlights: A high Thermoelectric Performance ZT=1.4 is gained for the Polycrystalline $In_4Se_{2.5}$ by Multiple Heteroatoms Induced Carrier Engineering and Hierarchical Nanostructure.

Colour graphic: